Hindawi
Advances in Materials Science and Engineering
Volume 2023, Article ID 6020950, 7 pages
https://doi.org/10.1155/2023/6020950

Research Article

Preparation and Adsorption Performance on Congo Red of Sodium Alginate-Lanthanum Hydrogel Spheres

Dan Dang,[1] **Mei Lei**,[2] **Xinyi Jiang**,[1] **Rui Song**,[1] **Gaimeng Yan**,[1] **and Wenju Liu**[1]

[1]*School of Chemistry and Chemical Engineering, Henan University of Technology, Zhengzhou 450001, China*
[2]*State Power Investment Corporation Science and Technology Research Institute Co., Ltd., South of Park Future Science City, Changping District Beijing, Beijing 100029, China*

Correspondence should be addressed to Wenju Liu; wenjuliu@haut.edu.cn

Received 5 May 2023; Revised 28 October 2023; Accepted 17 November 2023; Published 27 November 2023

Academic Editor: Hany Abdo

Sodium alginate-lanthanum (SA/Lan) hydrogel spheres were prepared by ion cross-linking method to remove Congo Red (CR) in an aqueous solution. The adsorption performance was assessed through batch experiments. The experiment revealed that the highest adsorption capacity of SA/Lan for CR was achieved when the mass concentration of La^{3+} was 1%, the dosage was 2 $g{\cdot}L^{-1}$, the initial concentration of CR was 30 $mg{\cdot}L^{-1}$, the adsorption time was 60 min, and the reaction temperature was 25°C. The adsorption capacity of 10.81 $mg{\cdot}g^{-1}$ was the corresponding figure. The adsorption process was consistent with the Langmuir and pseudosecond-order models.

1. Introduction

The use of dyestuff in textile and paper industries has led to the discharge of large amounts of dyestuff wastewater during their manufacturing and use [1]. The high chromaticity and difficult biodegradability of these dyestuffs render their degradation challenging, and some dyestuffs have been shown to produce carcinogenic and teratogenic substances upon contact with the human body, posing a threat to both the ecological environment and human health [2–5]. Among the various treatment methods for dye wastewater, adsorption is a popular option due to its simplicity, economic efficiency, and recyclability [6]. However, the commonly used adsorbents such as activated carbon [7, 8] and nanomaterials [9] are difficult to separate from wastewater, often causing secondary pollution, and hindering the overall environmental protection effort [10, 11].

Hydrogels are a type of three-dimensional network-structured gels with exceptionally high hydrophilicity and a vast specific surface area that encompasses a large number of functional groups [12]. This structure makes them ideal for removing different types of pollutants from wastewater. Sodium alginate (SA), as a biomass material, has outstanding qualities for efficient water treatment, such as biocompatibility, renewability, degradability, recyclability, and eco-friendliness. It is widely used as a biosorbent because it is rich in carboxyl and hydroxyl groups and has a high affinity for various multivalent metal ions and dyes [13]. Han et al. developed stable porous hydrogels made of carboxymethyl chitosan/formic acid (CMCS-PA), where CMCS-PA (3 : 1) composite hydrogels at pH = 7 at room temperature delivered excellent results on the removal of methyl orange [14]. Meanwhile, Xu et al. produced a composite hydrogel using AOPIM/Alg that could effectively remove cationic dyes from aqueous solutions, and its adsorption capacity on neutral red could reach 182 $mg{\cdot}g^{-1}$ [15]. Additionally, Li's study reported the preparation of a calcium alginate porous membrane with exceptional adsorption capacity, reaching 1679.52 $mg{\cdot}g^{-1}$ at the equilibrium concentration of methylene blue of 80 $mg{\cdot}L^{-1}$ at 15°C. This membrane also has a reliable recycling and regeneration capacity, making it a realistic choice for the treatment of wastewater.

In the area of hydrogel-mediated adsorption of dyes, the majority of studies have focused on cationic dyes, with far fewer investigations into anionic dyes. Litefti et al. [16] adsorbed CR using by-products of the wood industry with a CR adsorption of 0.50 mg/g, which was too long for the CR

removal cycle. Abbasi et al. [17] used lanthanum-doped bismuth ferrite calixarenes (BFOs) for their modification and adsorption of CR. However, due to the inherent problems such as the formation of a secondary crystalline phase from the preparation of the BFOs, their practical utilization was limited.

To address this research gap, this study aims to prepare and optimize SA/Lan hydrogel spheres through ionic cross-linking. Lanthanum doping optimizes its surface properties and increases its surface charge. We systematically investigate the key factors affecting the adsorption performance of these hydrogel spheres, including the initial concentration of Congo Red (CR), dosage, temperature, and time. The synthesized SA/Lan adsorbs CR through abundant active sites and surface charge, and we aim to comprehend the process of adsorption by utilizing kinetic modeling and analyzing adsorption isotherms. Through this systematic study, we aim to provide a reliable basis for the treatment of anionic printing and dyeing wastewater. Its simultaneous high cleanliness, low cost, and ease of preparation give it a good prospect for industrial adsorption of Congo Red dye.

2. Experimental Section

2.1. Materials. Sodium alginate (SA) analytical reagent, Zhengzhou Piney Chemical Reagent Factory; anhydrous calcium chloride analytical reagent, Tianjin Kermel Chemical Reagent Co., Ltd.; lanthanum chloride heptahydrate, Shanghai Yi'en Chemical Technology Co., Ltd.; Congo Red (CR), Tianjin Kermel Chemical Reagent Co., Ltd. were used. Except for the labeled, all are the analytical reagents, and water used in the experimental processes was deionized water.

2.2. Preparation of Hydrogel Spheres. Here is a revised version of the paragraph with improved logical accuracy, detail, and academic style: to prepare SA/Lan hydrogel spheres of varying La^{3+} concentrations, a solution was prepared by dissolving 2 g of sodium alginate in 98 mL of deionized water and stirred magnetically at 80°C until fully dissolved. The resulting solution was then slowly added dropwise to a constantly pressure-separated funnel containing 0.1 to 10 wt. % lanthanum chloride in an aqueous solution. The mixture was left to rest and cross-link for 24 hours. The resulting hydrogel spheres were named SA/La3 (where "*n*" represents a 3.0 wt.% La^{3+} concentration, for example). Next, the hydrogel spheres were rinsed with deionized water 3 to 5 times and dried by wiping with lens paper.

2.3. Material Characterization. Transform infrared spectrometer (FT-IR, Perkin Elmer Frontier), Perkin Elmer Instruments (Shanghai) Co., Ltd.; scanning electron microscope (BET, Mac 2460), Micromeritics APSP, USA; and environmental scanning electron microscope (ESEM, QUANTA200), Guangzhou Beto Science & Technology Co., were used to characterize the materials.

2.4. Absorption Experiments. A certain quality of SA/Lan hydrogels (0.5 g·L^{-1} to 6.0 g·L^{-1}) was placed in a 150 mL flask. 50 mL of Congo Red dissolved at an initial concentration of 30–60 mg/L was added at pH 7 ± 0.5, which was put in a thermostatic shaker (25°C, 35°C, and 45°C) at a speed of 200 rpm for some time (5 min to 180 min). The residual solution of CR was measured by UV-Visible spectrophotometer, and adsorptive capacity was calculated using the following equation:

$$q = \frac{(c_0\text{-}c) * V}{m}, \tag{1}$$

where q is the adsorptive capacity (mg·g^{-1}), c_0, c are the initial concentration and the final concentration of CR solution (g·L^{-1}), V is the volume of CR solution (mL), and m is the dosage of SA/Lan hydrogel spheres.

3. Results and Discussion

3.1. Material Characterization. Figures 1 and 2 indicate the ESEM images (Environmental Scanning Electron Microscope, QUANTA200, Guangzhou Betop Scientific Ltd.) of the outside surface and cross section of the SA/La1 hydrogel spheres, respectively. Figure 1 shows that the surface of the SA/La1 hydrogel spheres was rough, and the uneven cross-linking of La with hydroxyl groups led to the formation of a large number of grooves and wrinkles, which provided more active sites and effectively improved their adsorption capacity [18–20]. As shown in Figure 2, the ESEM map presents a three-dimensional mesh structure with interconnected skeletal structures constituting numerous nanometer- and micrometer-scale pores, and this physically and chemically cross-linked network facilitates the exposure of a large number of binding sites, as well as the mass transfer of lanthanum and dyes to promote the removal process of pollutants [13]. However, with an average pore size of 0.7718 nm, the access of dyes to the interior may be limited. The SA/La1 hydrogel spheres have good adsorption space inside the sparse and porous interior, which provides the possibility for the next step of sparing and expanding the pores to improve the internal adsorption performance.

Table 1 shows the specific surface area data (BET, Mac2460) of SA/La1 hydrogel spheres. It is clear that the specific surface area of the gel spheres is small and their superior adsorption performance depends on the abundance of functional groups on the external surface.

Figure 3 shows the infrared spectrum (FT-IR, Perkin Elmer Frontier, Shanghai) of SA/La1 hydrogel spheres. It indicates that 3415 cm^{-1} is the stretching vibration peak of the –OH group [21]; the peaks at 1615 cm^{-1} and 1426 cm^{-1} are the antisymmetric stretching vibration peak and the symmetric vibration absorption peak of carboxylic acid COO–, respectively [22]; the peaks at 1085 cm^{-1} and 1034 cm^{-1} are associated with C-O stretching in acids, phenols, ethers, and esters [23, 24]. The wide range of functional groups on the surface of the hydrogel spheres provides a wealth of active sites for the adsorption of Congo Red.

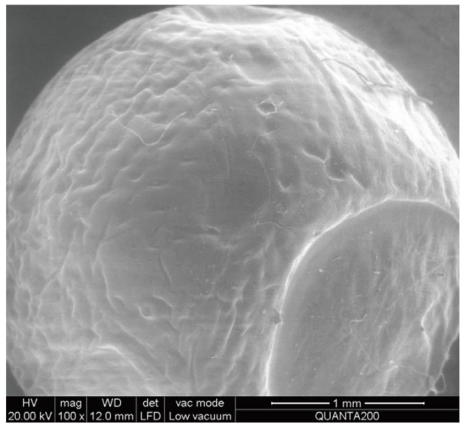

Figure 1: The outside surface of the SA/La1 hydrogel sphere.

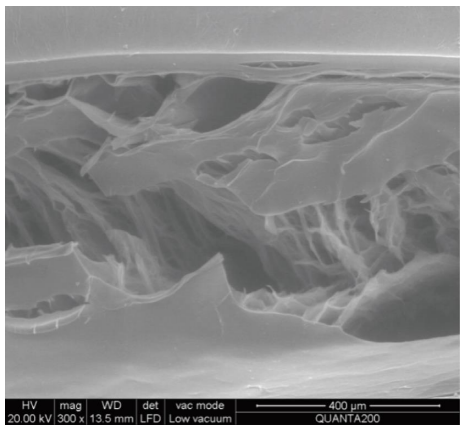

Figure 2: SA/La1 hydrogel sphere cross section.

Table 1: Specific surface area parameters of SA/La1 hydrogel spheres.

Sample	SA/La1 hydrogel spheres
Specific surface area ($m^2 \cdot g^{-1}$)	0.321
Total pore volume ($mm^3 \cdot g^{-1}$)	0.0620
Average pore size (nm)	0.772

3.2. Effect of La^{3+} Concentration of SA/Lan Hydrogel Spheres. A series of SA/Lan hydrogel spheres were prepared by sodium alginate cross-linking with lanthanum chloride solution using La^{3+} concentration of 0.1 to 10 wt.%. 2 $g \cdot L^{-1}$ SA/Lan hydrogel spheres were added to 30 $mg \cdot L^{-1}$ of CR solution shaking for 4 h. As shown in Figure 4, the doping of La ions is useful for the removal of CR [25]. The adsorption of CR is very low when not doped with La. The adsorption capacity of SA/Lan hydrogel spheres increased dramatically with the rise of the La^{3+} concentration before 1.0 wt. % of La^{3+} concentration. It is because La ions cross-link with carboxyl groups to optimize the surface properties and increase the surface positive charge of the hydrogel, enhancing the adsorption of CR. The La cross-linking saturated and then the adsorption capacity remained stable after the adsorption capacity reached 11.63 $mg \cdot g^{-1}$. So, 1 wt. % of La^{3+} concentration was selected for the preparation of hydrogel spheres in subsequent experiments.

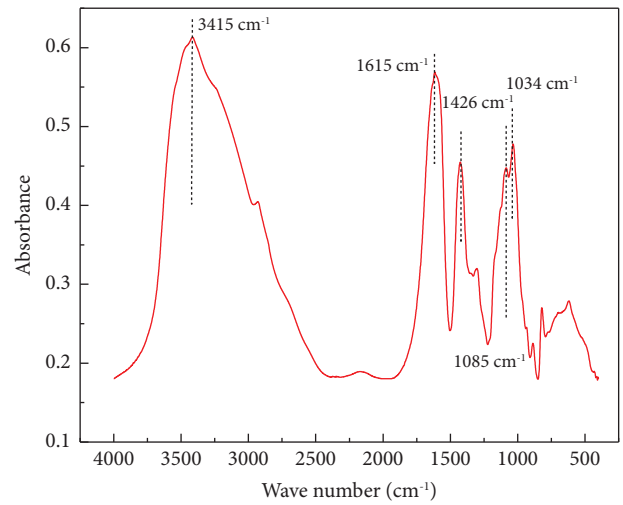

Figure 3: FT-IR of SA/La1 hydrogel spheres.

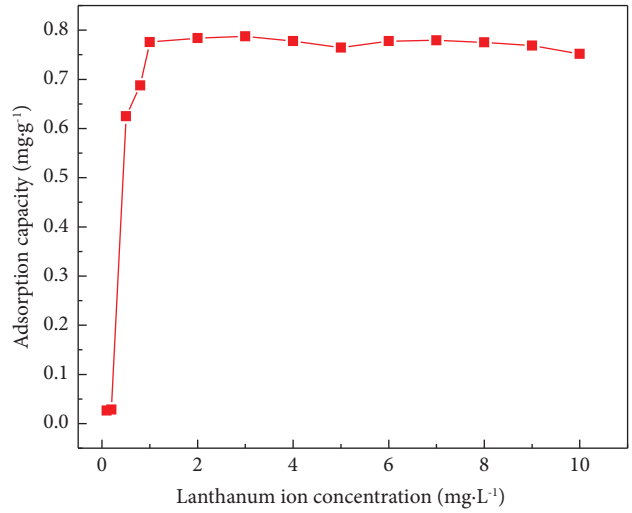

Figure 4: Effect of La^{3+} concentration on the preparation of SA/Lan hydrogel spheres.

3.3. Effect of Adsorption Time. 2 $g \cdot L^{-1}$ of SA/La1 hydrogel spheres was placed in 30 $mg \cdot L^{-1}$ of CR solution at 25°C for 5 min to 180 min. As shown in Figure 5, the adsorption capacity of SA/La1 hydrogel spheres increased rapidly before 60 min and reached adsorption equilibrium after 60 min, which is of great importance in such a short time to achieve equilibrium in practical applications. The equilibrium adsorption capacity of SA/La1 hydrogel spheres attained 10.81 $mg \cdot g^{-1}$ at 60 min.

3.4. Effect of Adsorbent Dosage. A certain dosage of SA/La1 hydrogel spheres was placed in 30 $mg \cdot L^{-1}$ of CR solution at 25°C for 60 min. As shown in Figure 6, when the initial concentration was 30 $mg \cdot L^{-1}$, the dosage of SA/La1 hydrogel spheres increased from 0.5 $g \cdot L^{-1}$ to 2 $g \cdot L^{-1}$. The adsorption capacity saw an increase from 5.32 mg g^{-1} to 9.17 mg g^{-1}, which is likely attributed to the addition of the adsorbent. This addition resulted in an increase in active adsorption

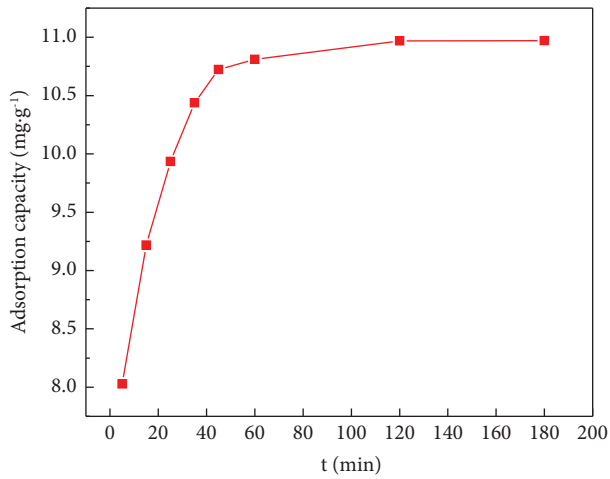

Figure 5: Effect of adsorption time on adsorption capacity of SA/La1 hydrogel spheres.

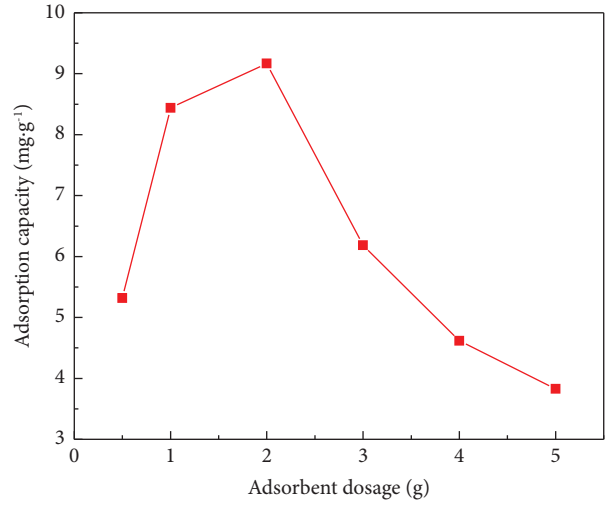

Figure 6: Effect of dosage on adsorption capacity of SA/La1 hydrogel spheres.

sites, thereby enhancing the adsorption capacity. Followed by, the adsorption capacity decreased as adsorbent was continuously added. The possible reason is that the adsorption of CR solution reaches equilibrium [22]. Unsaturated sites during adsorption lead to an increase in adsorption capacity with decreasing dosage as well as excess adsorbent required for the adsorption of dyes leading to a decrease in adsorption [26]. Therefore, the optimal input of the adsorbent was 2 g·L^{-1}.

3.5. Adsorption Kinetics. The interaction between dye molecules and the adsorbent was accompanied by studying the kinetics isotherms of adsorption behavior on the SA/La1 hydrogel spheres. The pseudofirst- and pseudosecond-order kinetic models were used to describe the kinetics isotherms of CR adsorption on the adsorbent respectively [27].

The pseudofirst-order kinetic equation is

$$\ln(q_e\text{-}q_t) = \ln q_e\text{-}K_1 t. \quad (2)$$

The pseudosecond-order kinetic equation is

$$\frac{t}{q_t} = \frac{1}{q_e{}^2 K_2} + \frac{t}{q_e}, \quad (3)$$

where q_e is the adsorption capacity at equilibrium (mg g^{-1}), q_t is the adsorption capacity at time (mg g^{-1}), K_1 is the rate constant of the pseudofirst-order kinetic model at equilibrium (min^{-1}), t is the adsorption time (min), and K_2 is the rate constant of the pseudosecond-order kinetic model at equilibrium (g·mg^{-1}·min^{-1}).

The entire adsorption process can be divided into two stages: during the initial stage, the adsorption rate is rapid. The adsorption capacity of CR on SA/La1 hydrogel spheres has reached 95% of the equilibrium adsorption capacity until adsorbing for 35 min. As the extension of adsorption time, the adsorption capacity gradually reaches the equilibrium state after 60 min. This may be attributed to the abundance of available active sites on the surface of SA/La1 hydrogel spheres during the initial stage. Moreover, the difference of concentration between the liquid phase and solid phase surface CR is large, meaning the adsorption driving force is big, which makes CR diffuse on the surface of the hydrogel sphere for reaction rapidly resulting in the adsorption rate increasing obviously. As the adsorption progresses, the active sites on the surface of the adsorbent gradually decrease, which causes a decrease in the adsorption rate until equilibrium.

Figure 7 and Table 2 display that the pseudosecond-order kinetic model is more suitable for describing the CR adsorption on SA/La1 hydrogel spheres as the R^2 of this model is 0.9999. It indicates that the chemisorption dominates the adsorption process.

To further illustrate the diffusion mechanism, we used an intraparticle diffusion model and we tried to study the diffusion mechanism of CR adsorption on SA/La1 hydrogel spheres as shown in Figure 8. Attributed to the rough surface formed by the association of La with hydroxyl groups, which provides more active sites and promotes the diffusion of dyes on the surface, the CR solution diffuses rapidly on the surface of SA/La1 hydrogel. The adsorption capacity rises rapidly and then reaches the adsorption equilibrium, which is consistent with the data obtained from the characterization of SA/La1 hydrogel spheres.

The ion diffusion equation is

$$q_t = K_{\text{ipd}} t^{0.5} + c, \quad (4)$$

where q_t is the adsorption capacity at time (mg g^{-1}), t is the adsorption time (min), and K_{ipd} is intraparticle diffusion model constants (mg·g^{-1}·min$^{-0.5}$).

3.6. Adsorption Isotherms. The study of adsorption isotherms provided a more lucid comprehension of the distribution of dye molecules between the liquid phase and the adsorbent surface when the adsorption system is in equilibrium. To understand the CR adsorption on SA/La1 hydrogel spheres, Figure 9 shows the adsorption isotherms at 25°C, 35°C, and 45°C. The Langmuir isotherm model (4) and the Freundlich isotherm model (5) were used to correspond to the data [26].

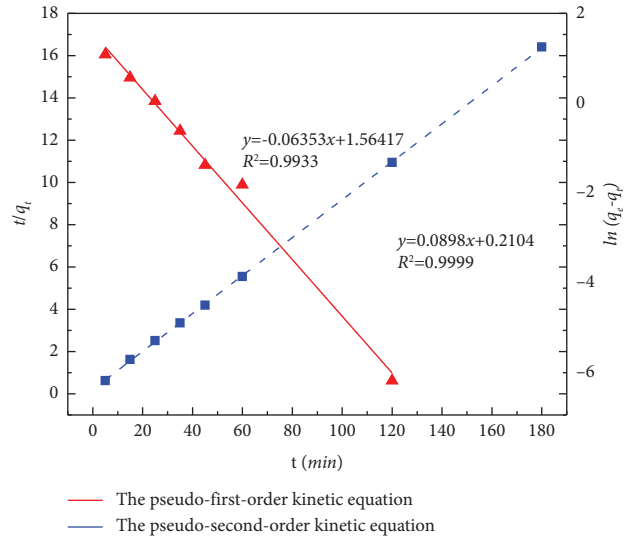

Figure 7: Kinetic curves of CR adsorption on SA/La1 hydrogel spheres.

Table 2: Fitting parameters of adsorption kinetics simulation.

Adsorbent	Experimental value	Pseudofirst-order kinetic model			Pseudosecond-order kinetic model		
	q_e (mg·g^{-1})	q_e (mg·g^{-1})	K_1 (min^{-1})	R^2	q_e (mg·g^{-1})	K_2 (g·mg^{-1}·h^{-1})	R^2
SA/La1	10.9699	4.7788	0.0635	0.9933	11.1359	0.0383	0.9999

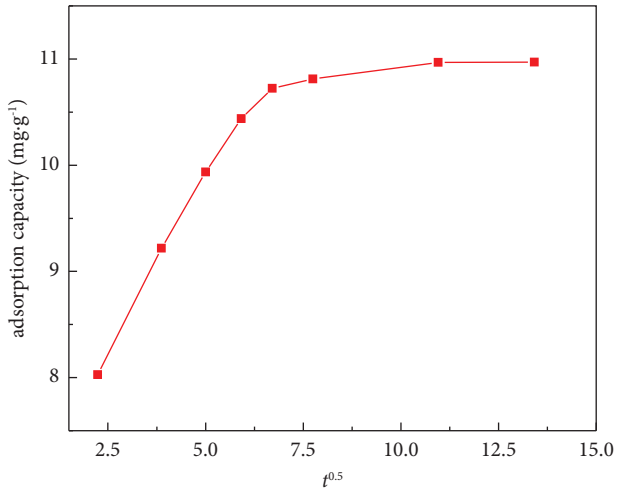

Figure 8: Fitting curve of the internal particle diffusion model.

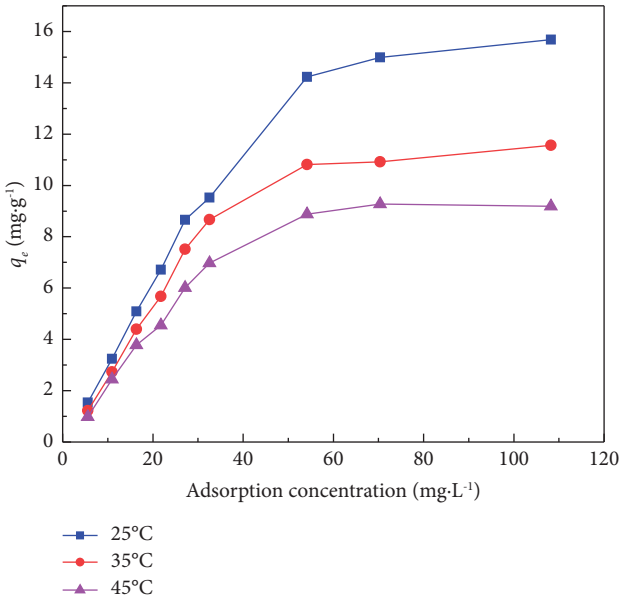

Figure 9: Adsorption isotherms of CR adsorption on SA/La1 hydrogel spheres.

The Langmuir isotherm equation is

$$\frac{c_e}{q_e} = \frac{c_e}{q_m} + \frac{1}{K_L q_m}. \quad (5)$$

The Freundlich isotherm equation is

$$\ln q_e = \ln K_F + \frac{1}{n} \ln c_e, \quad (6)$$

where c_e is the equilibrium concentration of CR in solution (mg·L^{-1}), q_e is the adsorption capacity at equilibrium (mg·g^{-1}), q_m is the maximum monolayer adsorption capacity (mg·g^{-1}), K_L is Langmuir adsorption equilibrium constant (L·mg^{-1}), K_F is Freundlich adsorption equilibrium constant (mg·L^{-1}), and n is the characteristic constant related to adsorption temperature.

As indicated in Table 3, the CR adsorption on SA/La1 hydrogel spheres at different temperatures can be described by Freundlich and Langmuir isotherm models. The R^2 value of the Langmuir model is closer to 1, and the maximum

Table 3: Adsorption isotherm equation fitting parameters of SA/La1 hydrogel spheres at different temperatures.

Temperature (°C)	Freundlich isotherm model			Langmuir isotherm model		
	n	K_F (mg·L^{-1})	R^2	q_m (mg·L^{-1})	K_L (L·mg^{-1})	R^2
25	1.5733	1.5336	0.8284	20.0803	0.0594	0.9345
35	1.5790	1.0745	0.8177	14.8368	0.0549	0.9356
45	1.5995	0.8463	0.8085	11.9189	0.0517	0.9208

adsorption capacity is 20.08 mg·g^{-1}. These results indicated that the Langmuir model more suitably described this system and its adsorption process belongs to single molecular layer adsorption.

4. Conclusions

SA/Lan hydrogel spheres were synthesized via ionic cross-linking, and their adsorption capacity for CR was investigated at various La^{3+} concentrations, with the highest performance observed for spheres containing 1 wt. % La^{3+}. The effects of adsorption time, dosage, and temperature on CR adsorption by SA/Lan hydrogel spheres were examined, with optimal performance achieved using 2.0 g·L^{-1} of spheres, at an initial CR concentration of 30 mg·L^{-1}, and reaction temperature of 25°C, for a 60 min adsorption time with an adsorption capacity of 10.81 mg·g^{-1}. The adsorption process of SA/Lan hydrogel spheres was observed to follow both the pseudosecond-order kinetic model and the Langmuir adsorption isotherm model. By this, we try to explain a possible chemisorption mechanism. The Langmuir model better fits the experimental data than the Freundlich model. SA/Lan hydrogel spheres have a uniform surface structure but a loose and porous interior. Therefore, further investigation of the expansion of surface pore size is necessary to enhance their adsorption performance. There is limited research on materials for adsorbing CR, and compared to other studies, SA/Lan's low cost, environmental friendliness, and enormous potential make it a suitable dye adsorbent for the industry.

Data Availability

The data used to support the findings of this study are available from the corresponding author upon request.

Conflicts of Interest

The authors declare that they have no conflicts of interest.

Acknowledgments

This work was supported by the Science and Technology Foundation of Henan Province (No. 232102320217).

References

[1] M. Premaratne, G. K. S. H. Nishshanka, V. C. Liyanaarachchi, P. H. V. Nimarshana, and T. U. Ariyadasa, "Bioremediation of textile dye wastewater using microalgae: current trends and future perspectives," *Journal of Chemical Technology and Biotechnology*, vol. 96, no. 12, pp. 3249–3258, 2021.

[2] D. Kurniawati, T. K. Sari, T. K. Sari, F. Adella, and S. Sy, "Effect of contact time adsorption of rhodamine B, methyl orange and methylene blue colours on langsat shell with batch methods," *Journal of Physics: Conference Series*, vol. 1788, no. 1, Article ID 012008, 2021.

[3] R. Wen, D. Zeng, Z. Yang et al., "Rapid analysis of illegal cationic dyes in foods and surface waters using high-temperature direct analysis in real-time high-resolution mass spectrometry," *Journal of Agricultural and Food Chemistry*, vol. 66, no. 28, pp. 7542–7549, 2018.

[4] D. Patel, S. L. Bapodra, D. Madamwar, and C. Desai, "Electroactive bacterial community augmentation enhances the performance of a pilot scale constructed wetland microbial fuel cell for treatment of textile dye wastewater," *Bioresource Technology*, vol. 332, Article ID 125088, 2021.

[5] Q. Feng, B. Gao, Q. Yue, and K. Guo, "Flocculation performance of papermaking sludge-based flocculants in different dye wastewater treatment: comparison with commercial lignin and coagulants," *Chemosphere*, vol. 262, Article ID 128416, 2021.

[6] U. O. Aigbe, K. E. Ukhurebor, R. B. Onyancha, O. A. Osibote, H. Darmokoesoemo, and H. S. Kusuma, "Fly ash-based adsorbent for adsorption of heavy metals and dyes from aqueous solution: a review," *Journal of Materials Research and Technology*, vol. 14, pp. 2751–2774, 2021.

[7] R. Jain, M. Mathur, S. Sikarwar, and A. Mittal, "Removal of the hazardous dye rhodamine B through photocatalytic and adsorption treatments," *Journal of Environmental Management*, vol. 85, no. 4, pp. 956–964, 2007.

[8] J. Song, Y. Li, Y. Wang et al., "Preparing biochars from cow hair waste produced in a tannery for dye wastewater treatment," *Materials*, vol. 14, no. 7, p. 1690, 2021.

[9] I. M. El-Sewify, A. Radwan, A. Shahat, M. F. El-Shahat, and M. M. Khalil, "Superior adsorption and removal of aquaculture and bio-staining dye from industrial wastewater using microporous nanocubic Zn-MOFs," *Microporous and Mesoporous Materials*, vol. 329, Article ID 111506, 2022.

[10] L. Bulgariu, L. B. Escudero, O. S. Bello et al., "The utilization of leaf-based adsorbents for dyes removal: a review," *Journal of Molecular Liquids*, vol. 276, pp. 728–747, 2019.

[11] S. Praveen, J. Jegan, T. Bhagavathi Pushpa, R. Gokulan, and L. Bulgariu, "Biochar for removal of dyes in contaminated water: an overview," *Biochar*, vol. 4, no. 1, p. 10, 2022.

[12] J. Cai, D. Ye, Y. Wu, L. Fan, and H. Yu, "Injectable alginate fibrous hydrogel with a three-dimensional network structure fabricated by microfluidic spinning," *Composites Communications*, vol. 15, pp. 1–5, 2019.

[13] Y. Feng, H. Wang, J. Xu et al., "Fabrication of MXene/PEI functionalized sodium alginate aerogel and its excellent adsorption behavior for Cr (VI) and Congo Red from aqueous solution," *Journal of Hazardous Materials*, vol. 416, Article ID 125777, 2021.

[14] D. Han, H. Zhao, L. Gao et al., "Preparation of carboxymethyl chitosan/phytic acid composite hydrogels for rapid dye adsorption in wastewater treatment," *Colloids and*

Surfaces A: Physicochemical and Engineering Aspects, vol. 628, Article ID 127355, 2021.

[15] S. Xu, Y. Jin, R. Li, M. Shan, and Y. Zhang, "Amidoxime modified polymers of intrinsic microporosity/alginate composite hydrogel beads for efficient adsorption of cationic dyes from aqueous solution," *Journal of Colloid and Interface Science*, vol. 607, pp. 890–899, 2022.

[16] K. Litefti, M. Stitou, M. Stitou, and J. G. Álvarez, "Adsorption of an anionic dye (Congo red) from aqueous solutions by pine bark," *Scientific Reports*, vol. 9, pp. 1–11, 2019.

[17] M. A. Abbasi, A. Rehman, Z. Ali, M. Atif, Z. Ali, and W. Khalid, "Congo red removal by lanthanum-doped bismuth ferrite nanostructures," *Journal of Physics and Chemistry of Solids*, vol. 170, Article ID 110964, 2022.

[18] J. H. Min and J. G. Hering, "Arsenate sorption by Fe(III)-DopedAlginate gels," *Water Research*, vol. 32, no. 5, pp. 1544–1552, 1998.

[19] X. W. Shi, Y. M. Du, L. P. Sun, J. H. Yang, X. H. Wang, and X. L. Su, "Ionically crosslinked alginate/carboxymethyl ChitinBeads for oral delivery of protein drugs," *Macromolecular Bioscience*, vol. 5, no. 9, pp. 881–889, 2005.

[20] X. Li, Y. Qi, Y. Li, Y. Zhang, X. He, and Y. Wang, "Novel magnetic beads based on sodium alginate gel crosslinked by zirconium(IV) and their effective removal for Pb2+ in aqueous solutions by using a batch and continuous systems," *Bioresource Technology*, vol. 142, pp. 611–619, 2013.

[21] M. K. Zhang, X. H. Zhang, and G. Z. Han, "Magnetic alginate/PVA hydrogel microspheres with selective adsorption performance for aromatic compounds," *Separation and Purification Technology*, vol. 278, Article ID 119547, 2021.

[22] G. Zhou, J. Luo, C. Liu, L. Chu, and J. Crittenden, "Efficient heavy metal removal from industrial melting effluent using fixed-bed process based on porous hydrogel adsorbents," *Water Research*, vol. 131, pp. 246–254, 2018.

[23] S. Thakur, S. Pandey, and O. A. Arotiba, "Development of a sodium alginate-based organic/inorganic superabsorbent composite hydrogel for adsorption of methylene blue," *Carbohydrate Polymers*, vol. 153, pp. 34–46, 2016.

[24] Y. Chen, L. Li, Y. Li et al., "Preparation of a double-network hydrogel based on wastepaper and its application in the treatment of wastewater containing copper (ii) and methylene blue," *RSC Advances*, vol. 11, no. 29, pp. 18131–18143, 2021.

[25] M. J. B. de Souza, T. R. S. Ribeiro, T. H. A. Silva, D. C. de Melo Silva, A. M. G. Pedrosa, and A. O. S. da Silva, "Study of liquid phase adsorption of Congo red on micro and mesoporous adsorbents containing lanthanum," *Materials Research Express*, vol. 6, no. 10, Article ID 105036, 2019.

[26] N. Beigi, H. Shayesteh, S. Javanshir, and M. Hosseinzadeh, "Pyrolyzed magnetic NiO/carbon-derived nanocomposite from a hierarchical nickel-based metal-organic framework with ultrahigh adsorption capacity," *Environmental Research*, vol. 231, Article ID 116146, 2023.

[27] H. Shayesteh, A. Rahbar-Kelishami, and R. Norouzbeigi, "Adsorption of malachite green and crystal violet cationic dyes from aqueous solution using pumice stone as a low-cost adsorbent: kinetic, equilibrium, and thermodynamic studies," *Desalination and Water Treatment*, vol. 57, no. 27, pp. 12822–12831, 2016.